Rapid and Versatile Photonic Annealing of Graphene Inks for Flexible Printed Electronics

Ethan B. Secor, Bok Y. Ahn, Theodore Z. Gao, Jennifer A. Lewis, and Mark C. Hersam*

The surging field of printed electronics offers a promising methodology for the fabrication of novel electronic devices,[1,2] which spans applications in energy conversion and storage,[3,4] flexible displays,[5] distributed sensor networks,[6] and intelligent and interactive packaging.[7] By integrating solution-processed electronic materials in high-throughput, low-cost manufacturing platforms, printed electronics is poised to have a growing impact on many technologies. The vision of inexpensive, large-area electronics is enabled by rapid, solution-phase processing techniques, epitomized by roll-to-roll manufacturing.[8] Drop-on-demand inkjet printing is an important capability for this field, offering additive, noncontact, and digital patterning capabilities. As such, there is strong demand to develop inkjet-printable inks based on high-performance electronic materials to expand the scope of possible applications for printed electronics. To date, a wide range of materials have been adapted to inkjet printing, including organic molecules and polymers, metallic and ceramic nanoparticles, carbon and post-carbon nanomaterials, and sol-gel metal oxides.[9–12] Of these, graphene-based inks offer a desirable combination of electrical conductivity, chemical and environmental stability, and mechanical flexibility, and have been exploited for a range of applications in energy,[13,14] sensing,[15–17] and electronics.[18–20] While several strategies have been presented for inkjet printing of graphene, they are limited in one or more of several key qualities, namely, high electrical conductivity, rapid printing and post-processing, and broad substrate compatibility.[12] Here, we concurrently achieve these requirements by coupling inkjet printing with intense pulsed light (IPL) annealing to achieve rapid fabrication of high conductivity graphene patterns on myriad substrates.

To realize this goal, we build from previous work demonstrating high performance inkjet-printed graphene,[21] reworking the graphene and ink production processes to enable rapid IPL annealing. Graphene is produced in gram-scale quantities by liquid phase exfoliation based on shear mixing in the presence of a polymer stabilizer, ethyl cellulose.[22,23] As shown in **Figure 1**a, the graphene flakes have a typical thickness of ≈2 nm and lateral area of ≈100 nm × 100 nm (detailed particle size distributions available in the Supporting Information, Figure S1). Flocculation of the graphene particles produces a graphene/ethyl cellulose composite powder, from which concentrated graphene inks are prepared for inkjet printing, as illustrated in Figure 1b. The polymer stabilizer enhances the ink stability and printing performance, but requires decomposition following printing to achieve optimal electrical properties.[14,21,24] While polymer decomposition has traditionally been achieved by thermal annealing, the high temperature and long duration required are incompatible with rapid processing and thermally sensitive substrates, such as poly(ethylene terephthalate) (PET) and poly(ethylene naphthalate) (PEN), which are desirable for printed electronics (Supporting Information, Figure S5). To address this issue, we explore the use of IPL annealing, a photonic technique commonly used to sinter metal nanoparticle inks, which offers rapid processing compatible with roll-to-roll manufacturing.[25–28] As illustrated in Figure 1c, this method uses a high-intensity pulsed xenon lamp to anneal the printed graphene patterns. Due to the large disparity in optical absorption between the graphene and the underlying substrate, photothermal heating occurs selectively in the printed film to minimize substrate damage. Through comprehensive optimization of the graphene production, ink formulation, and annealing conditions, we demonstrate effective IPL annealing of inkjet-printed graphene patterns, achieving significant and simultaneous advances in graphene ink loading, high-speed processing, and substrate versatility.

To investigate IPL annealing of inkjet-printed graphene patterns, we first explore the importance of the printed graphene film composition. In particular, the graphene:polymer ratio of the printed film is expected to influence the effectiveness of IPL annealing, because photonic annealing is commonly sensitive to the presence of additives in the ink formulation.[28] By changing the ethyl cellulose composition in the graphene exfoliation step, we obtain graphene/ethyl cellulose powders with a graphene composition ranging from 25 to 65 wt% as precursors for the graphene inks (details in the Experimental Section and the Supporting Information). These inks are prepared by dispersion of the graphene/ethyl cellulose powder in a solvent system composed of 85:15 v/v cyclohexanone/terpineol, used previously for high performance inkjet printing. To confirm the importance of the graphene composition for IPL annealing, films containing 25 and 50 wt% graphene are printed onto glass slides and PET foils for thermal and IPL annealing, respectively. For the films containing 25 wt% graphene, the sheet resistance is shown for thermal and IPL annealing in

E. B. Secor, T. Z. Gao, Prof. M. C. Hersam
Department of Materials Science and Engineering
Northwestern University
2220 Campus Drive, Evanston, IL 60208, USA
E-mail: m-hersam@northwestern.edu
Dr. B. Y. Ahn, Prof. J. A. Lewis
Harvard School of Engineering and Applied Sciences
Wyss Institute for Biologically Inspired Engineering
Cambridge, MA 02138, USA
Prof. M. C. Hersam
Department of Chemistry
Department of Medicine
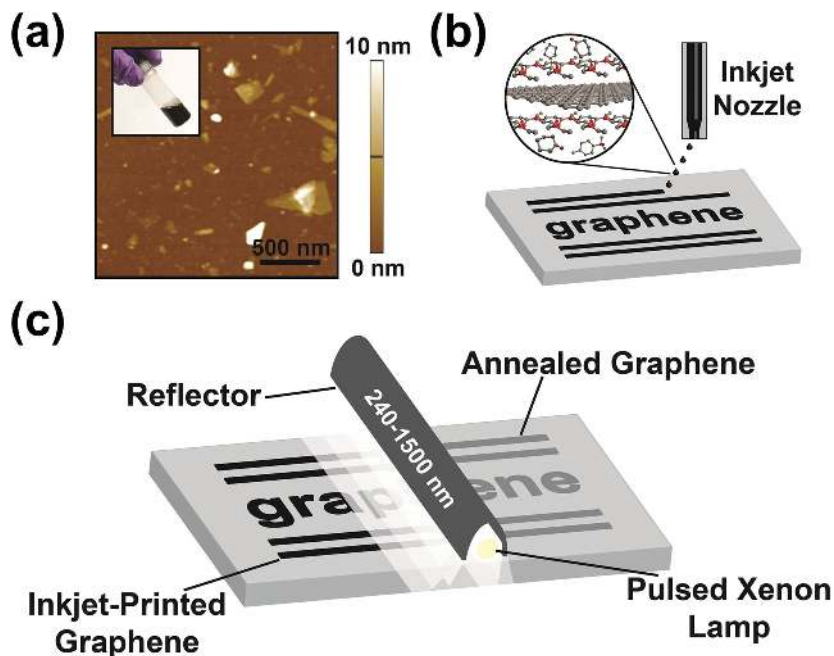Northwestern University
Evanston, IL 60208, USA

Figure 1. Inkjet printing and intense pulsed light (IPL) annealing of graphene. a) Atomic force microscopy image of graphene flakes; inset: image of graphene ink vial. b) Schematic illustration of inkjet printing of graphene. c) Schematic illustration of IPL annealing applied to graphene patterns.

The realization of IPL annealing for graphene films on PET suggests that this method can be generalized to other substrates. The sheet resistance as a function of light pulse energy is shown in **Figure 3**a for films on four different substrates, including PET, PEN, polyimide (PI), and glass, confirming the versatility of this method. Consistent with previous reports, we observe that the required pulse energy depends on the particular substrate due primarily to differences in substrate thermal properties.[28,31] While the low thermal conductivity and limited heat capacity of PET and PEN lead to highly conductive films for low energy light pulses, the somewhat thicker PI and much thicker glass require additional energy for comparable results. Notably, though, all substrates support graphene films with sheet resistance comparable to that achieved through thermal annealing. To further validate the versatility of this strategy, we printed individual lines on PET, PEN, PI, glass, and hexamethyldisilazane (HMDS)-treated glass to verify the well-behaved wetting and drying properties of the ink on each substrate. As
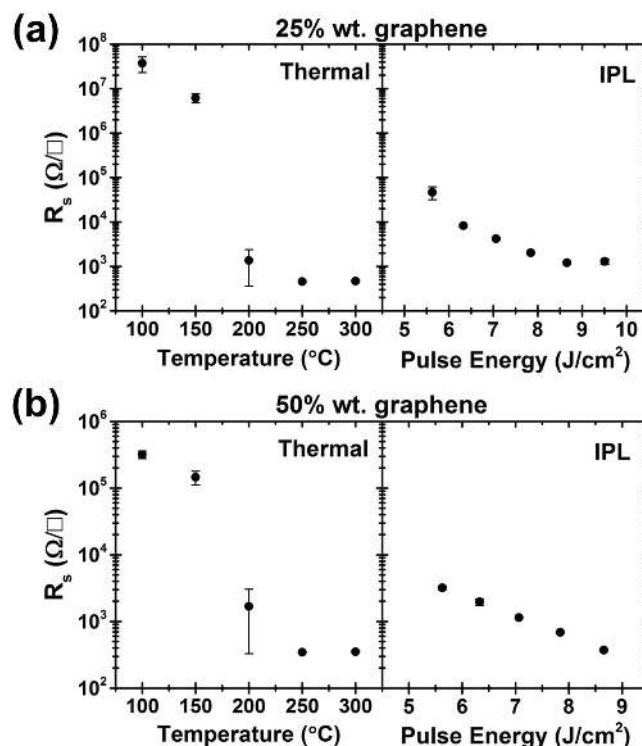
Figure 2a. Although photonic annealing is able to produce conductive films using pulse energies of 5–10 J cm^{-2}, the conductance of these films is a factor of ≈2.5 lower than that of optimized thermally annealed films of the same composition. Corresponding data for films containing 50 wt% graphene are shown in Figure 2b. In this case, IPL annealing produces films with a sheet resistance within 10% of the optimized thermally annealed samples. This low sheet resistance of IPL-annealed films containing 50 wt&% graphene demonstrates that IPL annealing is an effective post-processing strategy for this material system, even on temperature-sensitive substrates such as PET. In addition, comparison of the 25 and 50 wt% graphene films confirms that the effectiveness of IPL annealing depends on the graphene:polymer ratio of the printed films. Notably, a decrease in resistance is observed upon thermal annealing above a threshold temperature close to 200 °C due to decomposition of the polymer stabilizer (Supporting Information, Figure S2). While maintaining this high temperature is incompatible with many desirable substrates, IPL annealing can exceed this threshold temperature on a timescale short enough to promote polymer decomposition with minimal substrate damage,[28] leading to the gradual decrease in resistance with increasing annealing energy. Unlike prior work in which graphene oxide is reduced using light-based methods, graphene is already in a non-oxidized state.[23,29,30] We note that both thermal and IPL annealing result in similar evolution of the Raman spectra, namely, a reduction in the D to G band intensity ratio, I_D/I_G, for higher energy annealing (Supporting Information, Figure S7). A reduction in I_D/I_G is associated with reduced defect density and increasing graphitic nature for graphene particles and films, and is indicative of removal of the polymer binder.

Figure 2. Dependence of annealing on graphene:polymer ratio of the films. a) Sheet resistance as a function of processing conditions for a film containing 25 wt% graphene for thermal (left) and IPL (right) annealing. b) Corresponding sheet resistance as a function of annealing conditions for a film containing 50 wt% graphene, showing improved effectiveness of IPL annealing.
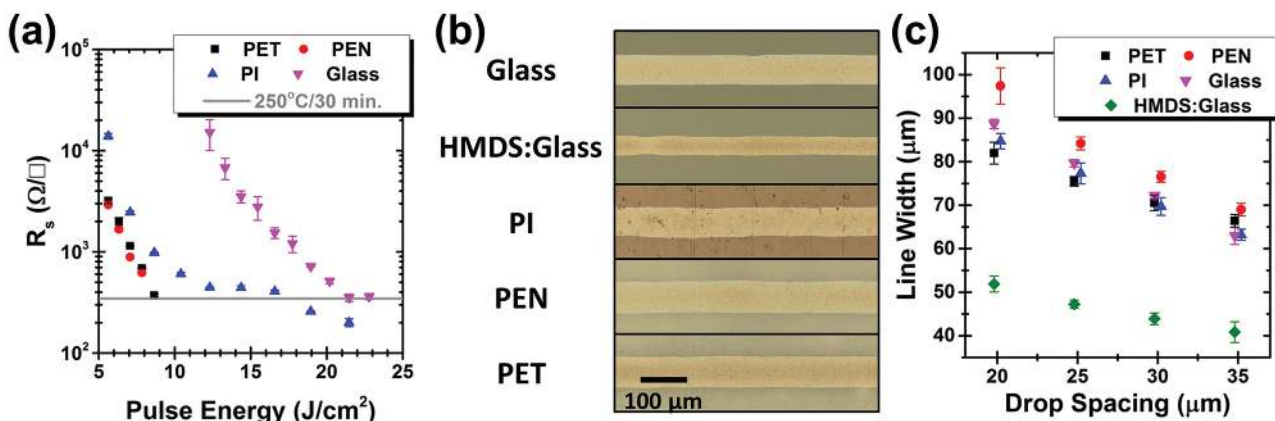
Materials
Views
www.MaterialsViews.com

ADVANCED
MATERIALS
www.advmat.de

COMMUNICATION

Figure 3. Versatility of IPL annealing for graphene patterns. a) Sheet resistance of graphene films as a function of annealing voltage, for different substrates (PET, PEN, PI, and glass). b) Optical microscopy images of lines on five different surfaces with a drop spacing of 35 μm, showing high-fidelity, uniform pattern definition. c) Resolution of inkjet-printed lines on the five surfaces as a function of drop spacing.

shown in Figure 3b, we observe highly uniform lines, with well-defined edges and negligible evidence of coffee ring formation, which is attributed to the ink composition, as discussed previously.[21] Figure 3c shows the line resolution on each substrate as a function of the droplet spacing. As expected, the line width decreases with increasing drop spacing, and behaves similarly on untreated substrates. When the substrate surface energy is tuned, as in the case of HMDS-treated glass, high-resolution lines can be obtained, with a line width below 50 μm. Overall, these results verify the suitability of our high-loading graphene ink for a range of substrates, both in terms of inkjet printing performance and compatible annealing.

While the enhanced graphene content of the ink is critical for optimal IPL annealing, it provides an additional benefit with respect to ink formulation. Specifically, graphene and other nanomaterial inks are typically characterized by a low concentration of active material.[11] This low nanomaterial content is a significant impediment for many practical applications, since the number of printing passes required to achieve a desired conductance, or thickness, scales inversely with the solids loading. In most cases, low concentrations are required to mitigate particle aggregation and achieve stable jetting. By contrast, ethyl cellulose acts as a highly effective stabilizer, allowing previously reported graphene concentrations as high as ≈3.4 mg mL^{-1} for inkjet printing and 80 mg mL^{-1} for screen printing.[21,32] As evidenced by the high concentration suitable for screen printing, the graphene loading for inkjet printing is not limited by particle stability, but instead by ink viscosity, which is typically in the range of 8–15 mPa s for inkjet printing.[11] For graphene/ethyl cellulose inks reported to date, the polymer component is the dominant contributor to the dispersion viscosity. Consequently, it follows that increasing the graphene content of the precursor powder offers a dual enhancement: a higher graphene concentration is achieved for the same total solids loading, and higher solids loading can be employed without exceeding the desirable viscosity range. To confirm this, a graphene ink was prepared using a 50 wt% graphene/ethyl cellulose powder, with a total solids loading of 4% w/v, yielding a total graphene concentration of 20 mg mL^{-1} at a

viscosity of 10–15 mPa s. By contrast, our previous ink based on 15 wt% graphene/ethyl cellulose powder exhibited a similar viscosity at 2.4% w/v solids loading, with a total graphene concentration of ≈3.4 mg mL^{-1}. In this manner, by controlling the solids loading and graphene:polymer ratio independently, we produce a graphene ink suitable for inkjet printing that is ≈6× more concentrated than previously demonstrated.

The high graphene concentration translates into thicker films for a given number of printing passes, ultimately reducing printing time. As shown in **Figure 4**a, the film thickness scales linearly with printing passes, with each additional pass adding 468 ± 5 nm in thickness prior to annealing, or 190 ± 6 nm in thickness following thermal annealing. This reduction in thickness is associated with decomposition of the polymer stabilizer and densification of the graphene network, consistent with previous reports.[33] As shown in Figure 4b, the sheet resistance decreases inversely with the number of printing passes, consistent with constant bulk conductivity. The conductivity for thermally annealed samples is measured to be 25 600 ± 900 S m^{-1}, even after a single printing pass. While the conductivity of IPL-annealed samples cannot be reliably measured due to changes in surface topography, the sheet resistance for IPL-annealed films is comparable to that of thermally annealed films, and decreases analogously for thicker films. It is therefore likely that IPL annealing will be effective for graphene/ethyl cellulose films deposited by other printing methods, such as gravure and screen printing,[32,33] because the primary difference between films deposited by these methods is the film thickness.

Altogether, our results represent a significant advance in the development of graphene inks for flexible printed electronics. IPL annealing allows rapid post-processing of graphene patterns, compatible with high-throughput roll-to-roll processing on a range of substrates. The combination of unprecedented graphene loading and high conductivity achieved for this ink offers a new route for high performance, printed electronics with clear advantages over competing graphene inks as well as other nonmetal conductors, e.g., reduced graphene oxide (RGO), carbon nanotubes (CNTs), and poly(3,4-ethylenedioxythiophene) polystyrene sulfonate (PEDOT:PSS). As
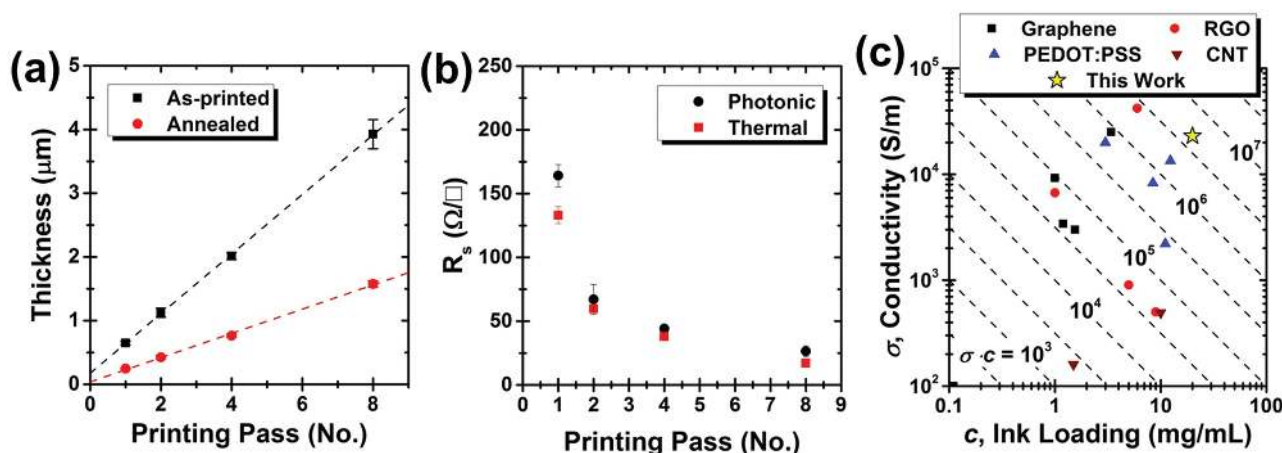
COMMUNICATION

Figure 4. Characterization of high concentration graphene inks. a) Thickness as a function of printing passes for graphene/ethyl cellulose films as-printed and following thermal annealing. Dashed lines indicate the least squares linear fit to the thickness data, indicating a thickness per pass of 190 nm following thermal annealing. b) Sheet resistance of graphene films at various thicknesses following thermal and IPL annealing, illustrating the suitability of IPL annealing over a broad range of film thickness. c) Map of ink concentration and conductivity for reported nonmetal conductive inkjet-printable inks, including inks based on graphene, RGO, CNTs, and PEDOT:PSS. The product of conductivity (σ) and concentration (c) is an indicator of the conductance achieved per printing pass, a key figure of merit for inkjet-printed conductors. Isolines for this metric are drawn as dashed lines to aid the eye.

previously suggested, a key figure of merit for practical applications is the conductance achieved per printing pass, which scales with the product of ink concentration and film conductivity. A range of competing conductive inkjet-printable inks is mapped out on axes of ink concentration and conductivity in Figure 4c, taken from the recent literature for graphene,[14,18,21,24,34] PEDOT:PSS,[35–38] RGO,[15,19,39] and CNTs (see the Supporting Information for details).[40,41] The dashed lines represent isolines of the product of conductivity and ink loading. Our graphene ink exhibits both high solids loading (20 mg mL^{-1}) and excellent conductivity (25 600 $\pm$ 900 S m^{-1}), with the product exceeding the value not only for competing graphene inks but also alternative inkjet-printed, nonmetal conductors. Moreover, graphene presents a number of additional desirable attributes, including robust chemical and environmental stability, reliable printability, and a well-defined chemistry without the need for harsh post-processing.

These excellent electrical properties, coupled with the intrinsic flexibility of graphene, motivate the application of graphene inks in flexible electronic circuitry, as illustrated in **Figure 5**a. It is therefore important to characterize the mechanical properties of IPL-annealed graphene films. While mechanical testing has been extensively performed for related graphene/ethyl cellulose inks following thermal annealing,[21] the fundamentally different conditions of IPL annealing can lead to distinct properties. Indeed, we note that films that are IPL annealed at high pulse energies exhibit different film morphologies from thermally annealed films (Supporting Information, Figure S8 and S9). A similar effect has been previously observed for metal nanoparticles sintered by IPL annealing, and is attributed to the extreme temperatures and heat gradients induced by the process.[42] In particular, the rapid polymer decomposition and generation of volatile products during IPL annealing could lead to local stresses,
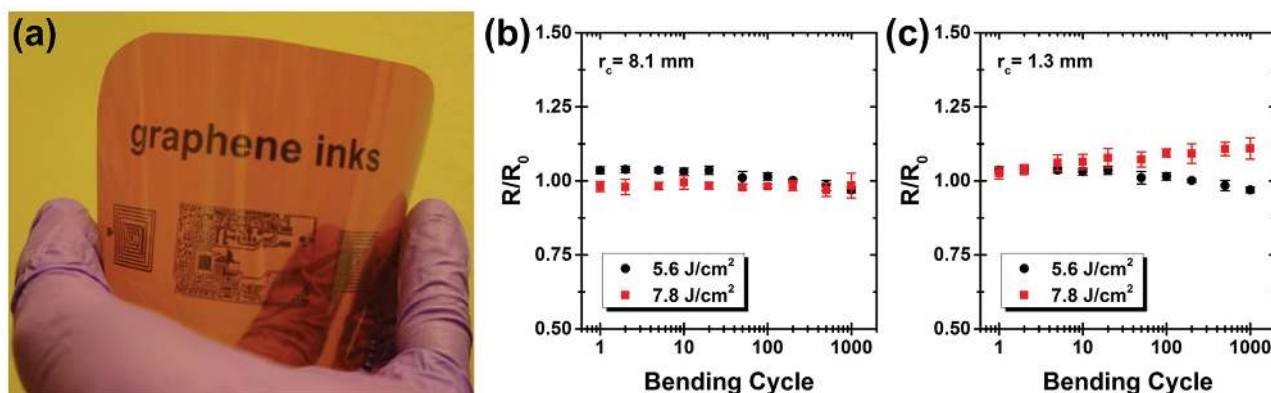

Figure 5. a) Large-area inkjet-printed graphene patterns on PI. b,c) Resistance measured as a function of bending cycles for graphene lines on PEN following IPL annealing at 5.6 and 7.8 J cm^{-2}, with bending radii of curvature of 8.1 and 1.3 mm, respectively (tensile strain of 0.0031 and 0.019, respectively).

resulting in the observed unique morphological features. In addition, although it is performed in ambient conditions, the rapid nature of IPL annealing can prevent oxidative processes, an effect widely exploited for processing copper-based inks.[43] Because oxygen is typically involved in thermal decomposition of ethyl cellulose, this effect could alter the fundamental nature of the annealing process.

To investigate the mechanical behavior of IPL-annealed graphene patterns, and thus confirm their suitability for flexible interconnects, we performed several bending tests. Specifically, graphene was inkjet printed onto PEN and processed by IPL annealing at two different pulse energies to produce conductive patterns. The electrical resistance of these stripes is measured over 1000 bending cycles to radii of curvature of 8.1 and 1.3 mm, as shown in Figure 5b,c. For the large radius of curvature, there is little discernible evolution of the line resistance. For the small bending radius test, the lower pulse energy produced lines with no deterioration upon bending, while the higher energy light pulse yielded lines with modest deterioration, exhibiting ~10% increase in resistance after 1000 bending cycles.

In summary, graphene is an attractive material for printed electronics, offering a chemically stable, mechanically flexible, and electrically conductive alternative to conventional metal nanoparticle and conductive polymer inks. The ink formulation, printing method, and rapid IPL annealing approach reported here overcomes several limitations of graphene inks to date, and is well suited for rapid, roll-to-roll fabrication of graphene patterns on myriad substrates. Furthermore, we leverage advances in ink formulation to produce highly concentrated inkjet-printable graphene inks, with a graphene concentration of 20 mg mL^{-1}. Overall, the high solids concentration, combined with the excellent conductivity of ≈25 000 S m^{-1} achieved after a single printing pass, establishes this graphene ink as a leading candidate for printed, flexible electronics.

Experimental Section

Liquid-Phase Exfoliation and Processing of Graphene: Graphene was exfoliated from graphite using a high shear mixer (Silverson L5M-A) with a square hole high shear screen. Ethyl cellulose (EC) (Sigma–Aldrich, 4 cP grade as measured at 5% in 80:20 toluene:ethanol, 48% ethoxy) was dissolved in ethanol (Koptec, 200 proof) at a concentration of 0.2–2% w/v (Supporting Information, Figure S2), and flake graphite (Asbury Graphite Mills, Grade 3061) was added at 10% w/v. This mixture was shear mixed for 2 h at 10 230 rpm in an ice bath, and then centrifuged at 4000 rpm (≈3000*g*) for 2 h to sediment out large graphite flakes (Beckman Coulter Avanti J-26 XPI centrifuge). The supernatant containing graphene, EC, and ethanol was harvested by pipette. For the flocculation step, this supernatant was mixed in a 16:9 wt. ratio with an aqueous NaCl solution (0.04 g mL^{-1} NaCl, Sigma–Aldrich, >99.5%) and centrifuged for 6 min at 7500 rpm (≈10 000*g*) to sediment the graphene/EC composite. This sediment was washed with deionized water, collected by vacuum filtration (Millipore Nitrocellulose HAWP 0.45 μm filter paper), and then dried to yield the graphene/EC powder, with a graphene content of 25–65 wt% depending on the starting EC loading (Supporting Information, Figure S2).

Ink Formulation and Preparation: Graphene/EC powder was directly dispersed in solvents for inkjet printing by bath sonication. The solvent system used for all inks in this study is 85:15 v/v cyclohexanone/terpineol (Sigma–Aldrich). For the initial study of the effect of graphene content and substrate dependence (Figure 2 and 3a), the inks contained 1% w/v graphene/EC powder comprised of 25 or 50 wt% graphene, as indicated. For the subsequent studies (Figure 3b,c– 5), the ink contained 4% w/v solids, based on a graphene/EC powder that contained 50 wt% graphene. All inks were filtered with a 3.1 μm glass fiber syringe filter following dispersion to prevent clogging of the inkjet nozzles. The filtered inks were briefly bath sonicated (5–10 min) prior to inkjet printing, and used over the course of four weeks to six months.

Inkjet Printing: All inkjet printing for this study was accomplished with a Ceradrop X-Serie inkjet printer equipped with a 10 pL nominal drop size Dimatix cartridge (DMC-11610). Printing was performed using a custom waveform modeled after the Dimatix Model Fluid 2 waveform at 1000–2000 Hz with the inkjet nozzle plate maintained at 30 °C and the substrate held at 35 °C. Printed patterns were dried at 80 °C for 60–180 min following printing to ensure complete solvent evaporation prior to annealing. Substrates for inkjet printing were obtained as follows: PET (Melinex ST579, 50 μm) and PEN (Teonex Q51, 50 μm) films were graciously supplied by DuPont Teijin Films; PI (DuPont Kapton, 125 μm) was purchased from American Durafilm; and 1 mm thick glass slides were purchased from VWR International. HMDS-treated glass slides were prepared using a vapor treatment technique. Glass slides were cleaned with acetone and isopropanol, and then subjected to O$_2$ plasma treatment for 5 min. They were then exposed to HMDS (Sigma–Aldrich, ≥99%) vapor at room temperature for 30 min, after which they were rinsed with isopropyl alcohol and dried under a N$_2$ stream. All other substrates were used as received. For the data presented in Figure 2 and 3a, the thickness of the graphene films corresponds to ≈80 nm following thermal annealing.

Intense Pulsed Light Annealing: IPL annealing was performed using a Xenon Sinteron 2000 with a pulse energy of 300–1500 J (see the Supporting Information for details). It is noted that the pulse energy indicated is the energy input of the lamp. A reasonable estimate is that ≈30% of the input energy is converted to radiation.[28] For all IPL annealing experiments, the sample was held a distance of 25 mm from the lamp, and 1 ms pulses were applied. In most cases (Figure 2b,d, 3a, and 5), a single light pulse was used. For thick films (Figure 4b, 2–8 layers), five light pulses were used with 5 s delay between each. Extensive data regarding sheet resistance for various annealing conditions are presented in the Supporting Information (Figure S10).

Characterization: The shear viscosity of the inks (Supporting Information, Figure S3) was measured with an Anton Paar Physica MCR 302 rheometer equipped with a 50 mm, 1° cone and plate geometry at shear rates of 1–1000 s^{-1}. The temperature was controlled by a Peltier plate. Printed line resolution measurements (Figure 3b,c) were obtained using an Olympus optical microscope, with the average and standard deviation plotted for 10 measurements at each condition. All electrical measurements were collected using a Keithley source meter. Film samples (Figure 2–4) were characterized using an in-line 4-point probe measurement system, taking into account appropriate geometric correction factors. Line samples (Figure 5) were analyzed using a two-probe measurement. Raman spectra were obtained using a Horiba Xplora Raman microscope equipped with a 532 nm laser. Peak intensity ratios (Supporting Information, Figure S7) indicate the average and standard deviation of five different spectra collected at different points. Note that a low laser power and long integration time were employed to avoid altering the sample from local heating. Measurements of the film thickness (Figure 4a) were collected on inkjet-printed films on glass using a Dektak 150 Stylus Surface Profiler.

Supporting Information

Supporting Information is available from the Wiley Online Library or from the author.

Acknowledgements

[1] D. Lupo, W. Clemens, S. Breitung, K. Hecker, in *Applications in Organic and Printed Electronics: A Technology-Enabled Revolution* (Ed: E. Cantatore), Springer, Boston, MA, USA **2013**, pp. 1–26.

[2] H. Sirringhaus, T. Kawase, R. H. Friend, T. Shimoda, M. Inbasekaran, W. Wu, E. P. Woo, *Science* **2000**, *290*, 2123.

[3] C. N. Hoth, S. A. Choulis, P. Schilinsky, C. J. Brabec, *Adv. Mater.* **2007**, *19*, 3973.

[4] A. M. Gaikwad, A. C. Arias, D. A. Steingart, *Energy Technol.* **2015**, *3*, 305.

[5] V. Wood, M. J. Panzer, J. Chen, M. S. Bradley, J. E. Halpert, M. G. Bawendi, V. Bulovic, *Adv. Mater.* **2009**, *21*, 2151.

[6] J. Jang, J. Ha, J. Cho, *Adv. Mater.* **2007**, *19*, 1772.

[7] V. Subramanian, J. M. J. Fréchet, P. C. Chang, S. Member, D. C. Huang, J. B. Lee, S. E. Molesa, A. R. Murphy, D. R. Redinger, S. K. Volkman, *Proc. IEEE* **2005**, *93*, 1330.

[8] R. R. Søndergaard, M. Hösel, F. C. Krebs, *J. Polym. Sci., Part B: Polym. Phys.* **2013**, *51*, 16.

[9] A. C. Arias, J. D. MacKenzie, I. McCulloch, J. Rivnay, A. Salleo, *Chem. Rev.* **2010**, *110*, 3.

[10] Y. Aleeva, B. Pignataro, *J. Mater. Chem. C* **2014**, *2*, 6436.

[11] A. Kamyshny, S. Magdassi, *Small* **2014**, *10*, 3515.

[12] E. B. Secor, M. C. Hersam, *J. Phys. Chem. Lett.* **2015**, *6*, 620.

[13] L. T. Le, M. H. Ervin, H. Qiu, B. E. Fuchs, W. Y. Lee, *Electrochem. Commun.* **2011**, *13*, 355.

[14] J. Li, F. Ye, S. Vaziri, M. Muhammed, M. C. Lemme, M. Östling, *Adv. Mater.* **2013**, *25*, 3985.

[15] L. Huang, Y. Huang, J. Liang, X. Wan, Y. Chen, *Nano Res.* **2011**, *4*, 675.

[16] V. Dua, S. P. Surwade, S. Ammu, S. R. Agnihotra, S. Jain, K. E. Roberts, S. Park, R. S. Ruoff, S. K. Manohar, *Angew. Chem. Int. Ed.* **2010**, *49*, 2154.

[17] D. Kong, L. T. Le, Y. Li, J. L. Zunino, W. Lee, *Langmuir* **2012**, *28*, 13467.

[18] F. Torrisi, T. Hasan, W. Wu, Z. Sun, A. Lombardo, T. S. Kulmala, G.-W. Hsieh, S. Jung, F. Bonaccorso, P. J. Paul, D. Chu, A. C. Ferrari, *ACS Nano* **2012**, *6*, 2992.

[19] Y. Su, J. Du, D. Sun, C. Liu, H. Cheng, *Nano Res.* **2013**, *6*, 842.

[20] S. Lim, B. Kang, D. Kwak, W. H. Lee, J. A. Lim, K. Cho, *J. Phys. Chem. C* **2012**, *116*, 7520.

[21] E. B. Secor, P. L. Prabhumirashi, K. Puntambekar, M. L. Geier, M. C. Hersam, *J. Phys. Chem. Lett.* **2013**, *4*, 1347.

[22] K. R. Paton, E. Varrla, C. Backes, R. J. Smith, U. Khan, A. O'Neill, C. Boland, M. Lotya, O. M. Istrate, P. King, T. Higgins, S. Barwich, P. May, P. Puczkarski, I. Ahmed, M. Moebius, H. Pettersson, E. Long, J. Coelho, S. E. O'Brien, E. K. McGuire, B. M. Sanchez, G. S. Duesberg, N. McEvoy, T. J. Pennycook, C. Downing, A. Crossley, V. Nicolosi, J. N. Coleman, *Nat. Mater.* **2014**, *13*, 624.

[23] Y. T. Liang, M. C. Hersam, *J. Am. Chem. Soc.* **2010**, *132*, 17661.

[24] Y. Gao, W. Shi, W. Wang, Y. Leng, Y. Zhao, *Ind. Eng. Chem. Res.* **2014**, *53*, 16777.

[25] K. A. Schroder, S. C. McCool, W. F. Furlan, *Tech. Proc. 2006 NSTI Nanotechnol. Conf. Trade Show* **2006**, *3*, 198.

[26] J. Perelaer, R. Abbel, S. Wünscher, R. Jani, T. van Lammeren, U. S. Schubert, *Adv. Mater.* **2012**, *24*, 2620.

[27] D. Angmo, T. T. Larsen-Olsen, M. Jørgensen, R. R. Søndergaard, F. C. Krebs, *Adv. Energy Mater.* **2013**, *3*, 172.

[28] S. Wunscher, R. Abbel, J. Perelaer, U. S. Schubert, *J. Mater. Chem. C* **2014**, *2*, 10232.

[29] L. J. Cote, R. Cruz-Silva, J. Huang, *J. Am. Chem. Soc.* **2009**, *131*, 11027.

[30] S.-H. Park, H.-S. Kim, *Nanotechnology* **2015**, *26*, 205601.

[31] J. Jiu, T. Sugahara, M. Nogi, T. Araki, K. Suganuma, H. Uchida, K. Shinozaki, *Nanoscale* **2013**, *5*, 11820.

[32] W. J. Hyun, E. B. Secor, M. C. Hersam, C. D. Frisbie, L. F. Francis, *Adv. Mater.* **2015**, *27*, 109.

[33] E. B. Secor, S. Lim, H. Zhang, C. D. Frisbie, L. F. Francis, M. C. Hersam, *Adv. Mater.* **2014**, *26*, 4533.

[34] D. Finn, M. Lotya, G. Cunningham, R. Smith, D. McCloskey, J. Donegan, J. N. Coleman, *J. Mater. Chem. C* **2014**, *2*, 925.

[35] Z. Xiong, C. Liu, *Org. Electron.* **2012**, *13*, 1532.

[36] P. Wilson, C. Lekakou, J. F. Watts, *Org. Electron.* **2013**, *14*, 3277.

[37] J. Ha, J. Park, J. Ha, S. Kim, S. Chung, C. Lee, Y. Hong, *Org. Electron.* **2015**, *19*, 147.

[38] B. Hu, D. Li, O. Ala, P. Manandhar, Q. Fan, D. Kasilingam, P. D. Calvert, *Adv. Funct. Mater.* **2011**, *21*, 305.

[39] K.-Y. Shin, J.-Y. Hong, J. Jang, *Chem. Commun.* **2011**, *47*, 8527.

[40] O. S. Kwon, H. Kim, H. Ko, J. Lee, B. Lee, C. H. Jung, J. H. Choi, K. Shin, *Carbon* **2013**, *58*, 116.

[41] S. Azoubel, S. Shemesh, S. Magdassi, *Nanotechnology* **2012**, *23*, 344003.

[42] D. J. Lee, S. H. Park, S. Jang, H. S. Kim, J. H. Oh, Y. W. Song, *J. Micromech. Microeng.* **2011**, *21*, 125023.

[43] H.-S. Kim, S. R. Dhage, D.-E. Shim, H. T. Hahn, *Appl. Phys. A* **2009**, *97*, 791.